Title

Side asymmetry in nasal resistance correlate with nasal obstruction severity in patients with septal deformities: computational fluid dynamics study

A short running title

Side asymmetry in nasal resistance and nasal airway obstruction in nasal septal deformities

Author full names

Nataša Janović[1], Aleksandar Ćoćić[2], Mirjana Stamenić[2], Aleksa Janović[3], Marija Djurić[1]

Affiliations

[1] Department of Anatomy, Laboratory for Anthropology, University of Belgrade, Faculty of Medicine, Belgrade, Serbia

[2] University of Belgrade, Faculty of Mechanical Engineering, Belgrade, Serbia

[3] Department of Diagnostic Radiology, University of Belgrade, Faculty of Dental Medicine, Belgrade, Serbia

Corresponding author

Aleksa Janovic, MD, PhD

Department of Diagnostic Radiology, University of Belgrade, Faculty of Dental Medicine

6 Rankeova, 11 000 Belgrade, Serbia

Tel/fax: +381 11 344 08 41, mail: aleksa.janovic@stomf.bg.ac.rs

Acknowledgments

We would like to express our gratitude and respect to recently deceased Professor Zoran Rakocevic for His invaluable help and support in the study conduction.

The authors acknowledge support from the Ministry of Education and Science of the Republic of Serbia, project number III45005.

Conflict of Interest

The authors have stated explicitly that there are no conflicts of interest in connection with this article.

Funding sources

None

Ethic Consideration

This study was conducted according to the Declaration of Helsinki, and approved by the Ethics Committee of the Faculty of Medicine, No. 29/V-1. All patients gave written informed consent to participate in the study.

DR ALEKSA JANOVIC (Orcid ID : 0000-0002-3084-0022)

Article type : Original Manuscript

Title

Side asymmetry in nasal resistance correlate with nasal obstruction severity in patients with septal deformities: computational fluid dynamics study

ABSTRACT

Objectives

The objective of this study was to investigate the relationship between side asymmetry in nasal resistance (NR) and severity of the nasal airway obstruction (NAO) in patients with different types of nasal septal deformity (NSD).

Design

Computational fluid dynamics (CFD) study

Setting

The study was conducted in a tertiary medical center

Participants

The study included 232 patients, who were referred to the CT examination of the paranasal sinuses. Exclusion criteria were sinonasal and respiratory diseases that may interfere

with the nasal obstruction. The presence and the type of NSD were recorded according to the Mladina's classification.

Main outcome measures

The presence and severity of NAO in each patient was assessed by NOSE questionnaire. Eight computational models of the nasal cavity were created from CT scans. Models represented seven Mladina's NSD types and a straight septum of a symptomless patient. CFD calculated airflow partitioning and NR for each nasal passage. Side differences in NR were calculated by the equation $\Delta NR = NR_{left} - NR_{right}$. The relationship between NOSE scores, airflow partitioning, and side differences in NR was explored using Spearman's correlation analysis.

Results

Mladina's types of NSD showed differences in airflow partitioning and the degree of side asymmetry in NR. A significant positive correlation was detected between side differences in NR and NOSE scores (R=0.762, *p=0.028*). A significant negative correlation was found between the percent of unilateral airflow and NR (R= -0.524, *p= 0.037*).

Conclusions

Our results demonstrated that side asymmetry in NR could explain differences in NAO severity related to the NSD type.

Keywords: Nasal septal deformity; Nasal airway obstruction; Airflow partitioning; Nasal resistance; NOSE scale; Computational fluid dynamics; Computer tomography.

Keypoints

- The relationship between side asymmetry in nasal resistance (NR) and severity of nasal airway obstruction (NAO) in patients with nasal septal deformity (NSD) is underinvestigated.

- The effect of different types of NSD to the side asymmetry in NR is not known.
- Computational fluid dynamics (CFD) analysis revealed a different degree of side asymmetry in NR between Mladina's types of NSD.
- The degree of side asymmetry in CFD-derived NR had a significant positive correlation with NOSE scores.
- We demonstrated that NSD related side asymmetry in CFD-NR could be responsible for the subjective sensation of NAO severity.

1. INTRODUCTION

An intriguing relationship between nasal septal deformity (NSD) and subjective perception of the nasal airway obstruction (NAO) has been attracting scientific attention for more than three decades. Numerous studies have investigated NSD at anatomical, clinical, and more recently computational fluid dynamics (CFD) level in order to identify any parameter(s) that would answer the question why structurally severe NSD may be symptomless, and, by contrast, why some patients with minor NSD may suffer from severe NAO.

Clinical studies that used rhinomanometry (RMM) in patients with NSD have linked NAO symptoms with altered nasal airflow resistance (NR). In vivo experiments revealed that artificially made NSD at various parts of the nasal cavity increases RMM-derived NR[1]. This finding was later supported by clinical studies that reported increased NR at the narrow side of the nasal cavity[2,3]. Additionally, NSD related increase in NR was found to be site-dependent. Even a small deflection of the nasal septum at the internal nasal valve (INV) region harshly raised NR, whereas more considerable deformations inside the bony cavum minimally affected NR[1,4,5]. A stronger connection was reported between NAO and unilateral RMM-NR than bilateral (total) NR[3].

Recent application of CFD analysis allowed more detailed insight into the airflow pressure distribution through the nasal cavity. CFD studies that simulated NSD revealed substantial alterations in pressure drop and CFD-derived NR. Briefly, NSD was found to cause

abrupt changes in the pressure drop pattern through the nasal passages[6,7], and an increase in NR at the narrow side[6-9]. These studies analyzed NR changes in structurally simple or artificially created NSDs, generally without a precise description of the NSD morphology. However, a relationship between CFD-derived NR and NAO severity was rarely investigated, mostly in cases pre- and post-septoplasty[10-12].

Concerning the morphological diversity of the NSD, this study aimed to investigate pressure drop patterns and NR in different NSD types using CFD analysis. Particular emphasis was on the relationship between side asymmetry in NR and NAO symptoms. We hypothesized that NSD related side differences in NR contribute to the subjective perception of the NAO severity.

2. MATERIALS AND METHODS

2.1. Ethical consideration

This study was conducted according to the Declaration of Helsinki, and approved by the Ethics Committee of the Faculty of Medicine, No. 29/V-1. All patients gave written informed consent to participate in the study.

2.2. Patient selection

Patients were selected prospectively among adults referred to the Department of Diagnostic Radiology due to computed tomography (CT) examination of the paranasal sinuses. Patients were considered eligible if they had a negative history of the following conditions: acute or chronic rhinosinusitis, nasal polyposis, turbinate hypertrophy, allergic rhinitis, sinonasal malignancy, radiation therapy, nasal surgery, facial bone trauma, developmental facial anomalies, and any respiratory disease that may interfere with the nasal obstruction. Among 450 consecutively examined patients, 232 met the inclusion criteria. All patients fulfilled the Nasal Obstruction Symptom Evaluation (NOSE) questionnaire and self-assessed nasal obstruction severity experienced during the last month[13].

Intranasal decongestants were administered 15 min before the CT examination in order to minimize the effect of the nasal cycle to the geometry of the nasal passages. Patients were

examined by Siemens Somatom Sensation 16 CT devise (Munich, Germany). Scanning was performed in a supine position in 3 mm thick axial sections parallel to the hard palate. Obtained raw data were further reconstructed into thinner sections of 0.75 mm using bone window settings. An experienced head and neck radiologist analyzed all CT scans, recorded the presence of the NSD, and classified NSD according to the Mladina's classification[14] (Table 1). The decision whether the SD belongs to the type 1 or type 2 was made based on the CT measured INV angle[15].

2.3. Generation of three dimensional (3D) computational models

Eight 3D computational models were created from 0.75 mm thick CT scans. The first model represented the nasal cavity of a symptomless patient with a straight septum, while the other seven models were the most representative cases for each NSD type. Types 1, 2, 3, and 5 were left-sided, whereas the type 6 NSD was right-sided. Type 4 had a right-sided anterior and left-sided posterior curvature. Type 7 was combined of left-sided type 2 and right-sided type 5. DICOM files were imported into 3D Slicer software (4.1.2, open-source, National Institute of Health) to generate anatomically accurate geometry of the nasal cavity. The nasal airspace was extracted automatically by selecting pixels with Hounsfield Units ranging from -1024 to -512.12. Segment editor was used to delineate nasal passages. Pixels selected outside the nasal passages were removed manually. The final 3D models included nasal passages from the nostrils to the oropharynx and were saved in *.stl files.

Before grid generation, eight section planes perpendicular to the air stream were defined through the nasal passages in order to comprehensively evaluate local changes in airflow pressure (Figure 1). In models containing a septal spur (type 5 and type 7), an additional cross-section was set at the most prominent point of the spur. The plane selection was made by CAD CAM software (CATIA V5R21, Academic licensed).

2.4. Grid generation

Stereolithography (*.stl) files were imported into cfMesh application within OpenFOAM software (version foam-extend 4.1) for automatic mesh generation[16]. Numerical meshes for all 3D models consist mostly of hexahedral elements, with three layers of boundary cells parallel to the cavity walls (boundary layer cells). The distance of 0.5mm from the wall is chosen as the

characteristic size of the first boundary layer cell. On average, the total number of cells for all models was around 5.5 million.

2.5. Boundary conditions

The inlet was set at the nostrils, while the outlet was placed in the nasopharynx. The walls of the nasal cavity were assumed rigid with a no-slip condition. A constant inspiratory flow rate of 125 mL/s[17] was set for both nostrils at the inlet, with a zero gradient at the outlet. Since the airflow was considered steady, a SIMPLE algorithm is used for pressure-velocity coupling. A laminar-transient-turbulent flow (k-ω SST model) was modeled in all cases with a low turbulence intensity of 2%[18]. It is assumed that simulations were converged when values of normalized residuals fall below 10^{-5}.

2.6. CFD analysis

After CFD simulations were run, the airflow distribution was calculated in each model as a percentage of a total inhaled air flowing through the right and left nasal passage, respectively. In order to analyze the pressure drop pattern, the mean pressure value was measured at eight segments along the nasal passages bilaterally (Figure 1).

Unilateral CFD-derived nasal resistance (CFD-NR) was calculated for the right and left nasal passage, respectively, using a standard equation $NR = \Delta p/Q$, where Δp represents a transnasal pressure drop between the inlet and choanae, and Q is a flow rate of 125 mL/s[12,19]. Side differences in the CFD-NR were calculated by the equation $\Delta NR = NR_{left} - NR_{right}$.

2.7. Statistical analysis

Statistical analysis was performed in SPSS for Windows, version 25.0 (SPSS, Inc., Chicago, IL). Descriptive statistical methods (mean, standard deviation) were applied to analyze the patient's NOSE scores in relation to the NSD type. The association between NOSE scores and CFD derived parameters (airflow partitioning and side differences in CFD-NR) was explored using Spearman's correlation analysis. The statistical significance was set at a level of 0.05.

3. RESULTS

3.1. NOSE scores

Table 2 displays patients' mean NOSE scores in the seven NSD types. Patients with NSD located in the INV region had the highest NOSE scores (types 2 and 1), followed by type 7 and 4. The lowest NOSE scores were recorded in type 6 and 3.

3.2. Side differences in airflow distribution

In the model without NSD and NAO, airflow was almost evenly distributed with a minimal difference between right and left nasal passage (Table 2). Side distribution of airflow in type 3, 4, 5, and 7 was similar to the model without NSD. More substantial alterations in the airflow partitioning between right and left nasal passages were observed in the NSD type 6, 1, and 2 with ascending order (Table 2).

3.3. Side differences in pressure drop and CFD-NR

Figure 2 illustrates the transnasal pressure drop through the right and left nasal passage in eight 3D models. In the model without NSD, similar pressure values were recorded on both sides, showing a smooth in-phase decrease along the nasal passages. CFD-NR, in the same model, also exhibits minimal side differences (Table 2). Transnasal pressure drop pattern in type 3 and 6 NSD models resembles that of a normal nasal cavity, including a constant in-phase decrease in pressure, minimal side differences in mean pressure values (Figure 2), and similar CFD-NR on each side (Table 2). Transnasal pressure drop in type 5 was similar to type 3, although side differences in the single pressure values in the anterior segments were slightly higher as well as the side difference in CFD-NR.

The appearance of pressure drop lines in other NSD models, however, revealed more accentuated side asymmetry in mean pressure values and CFD-NR (Table 2) including an out-of-phase pattern in a pressure drop (Figure 2). The largest side differences in the mean pressure values were observed in the anterior segments of the nasal cavity. In the segments behind, pressure continued to drop in-phase only in type 1. By contrast, types 2, 4, and 7 showed a steep initial drop in pressure at the narrow side, which subsequently increased to some extent in type 4 and 7. Almost a flat line in the pressure drop and low CFD-NR were noted in these three models in the opposite (wider) nasal passage. There were no detectable changes in the transnasal

pressure drop at the site of the bony spur in type 5 and 7 (Figure 2, segment 6 in NSD type 5 and 7).

3.4. Correlation between NOSE scale and CFD-deriver parameters

Statistical analysis confirmed a significant positive correlation between side differences in CFD-NR and mean NOSE scores (R=0.762, *p=0.028*). A significant negative correlation was detected between the percent of unilateral airflow and CFD-NR (R= -0.524, *p= 0.037*).

4. DISCUSSION

4.1. Synopsis of new findings

The current study revealed various degrees of side asymmetry in pressure drop and CFD-NR related to the NSD type. Based on our results, the highest side differences in CFD-NR exist in NSD located in the INV region (type 1, 2, 4, and 7). These differences were accompanied by the unequal side distribution of nasal airflow (Table 2), which was lower on the narrow side. Such a result is not unexpected since the INV area is the narrowest segment in the entire nasal cavity. Even a small narrowing in the INV area may increase NR and consequently, worse NAO[1,4,5]. Relatively small side differences in CFD-NR (slightly higher than the straight septum model) in type 6, 3, and 5 could be explained by NSD morphology. Type 3 and 5 are located in the posterior parts of the nasal cavity. Since the cross-sectional area in this part is much higher than in the anterior nasal cavity, inhaled air has enough space to bypass the narrow segment. Configuration of type 6 in our case did not cause significant side differences in the cross-sectional area and, subsequently, no significant effect on the NR side difference. More importantly, we demonstrated that NSD related side asymmetry in CFD-NR could be responsible for the subjective sensation of NAO severity.

4.2. Comparisons with other studies

Although experimental and clinical studies periodically reported side asymmetry in NR in patients with NSD[1,2,7,20,21], the clinical significance of this asymmetry has not been considered at all in the context of the NAO. Haavisto and Sipila[2] found that patient satisfaction following

septoplasty coincided with unilateral decrease in RMM-derived NR on the previously narrowed side. When looking at their results, one could notice a great side asymmetry in the mean RMM-NR before septoplasty that reduced significantly after surgery. Recent CFD studies of Rhee et al.[20,21] on pre and post-surgery NSD models contained similar findings. They found a great side asymmetry in CFD-NR in NSD models that normalized after septoplasty. The initial side asymmetry in airflow distribution showed the same trend after septoplasty. However, neither the side difference in CFD-NR was mentioned, nor its clinical impact on the NAO symptoms was discussed. More recently, Radulesco et al.[7] reported the presence of side differences in NR and airflow rate in patients with NSD without further interpretation or correlation with NAO symptoms. In light of our results, it seems that reduced side asymmetry in NR after septoplasty may better explain symptom improvement than an isolated decrease in unilateral NR on the narrow side.

4.3. Clinical applicability of the study

Nasal airflow in the right and left nasal cavity is normally asymmetrical in the healthy nose. This phenomenon, known as the nasal cycle, occurs due to spontaneous periodic fluctuations in NR that alternate air to flow from one nasal cavity to the other[22]. During a "working phase" of the nasal cycle, unilateral decongestion of erectile tissue in the nasal mucosa increases nasal width and decreases NR allowing the air to flow predominantly through this nasal cavity[22]. Simultaneously, the opposite side of the nose is in a "resting phase" that is characterized by erectile tissue congestion, nasal width reduction, NR increase, and consequent less air volume flowing through this side[22]. After several hours, the mucosal congestion and decongestion change sides allowing the resting side of the nasal cavity to start "work" and become dominant for breathing, while the previously working side is "resting". During the nasal cycle, unilateral NR may vary greatly, but the total NR remains relatively constant[23].

In a patient without NSD, a cyclic shifting of mucosal congestion/decongestion and consequent nasal airflow alteration between right and left nasal cavity occurs without any sensation. This function is under control of the autonomic nervous system and exists even in the absence of the nasal airflow, e.g., after laryngectomy[24,25]. The patient, therefore, is not aware of the unilateral periodic changes of the NR as long as there is a minimal side difference in NR that stays relatively constant over time[26]. In general, patients are not aware of the function of any

organ regulated by the autonomic nervous system, e.g., the heartbeat, until it becomes abnormal, such as in the case of arrhythmia. Similarly, if NR becomes highly asymmetrical between nasal passages for any reason, in this case, due to NSD, this may result in troublesome nasal breathing.

Side differences in CFD-NR in this study were obtained when airflow was simulated through both nasal passages simultaneously. Unlike previous CFD studies, we minimized the effect of the nasal cycle to NR by applying nasal decongestants before CT imaging. In fact, the presence of the nasal cycle might worse NAO symptoms. NR at the narrow side is always high regardless of the nasal cycle phase. Moreover, cyclic changes in NR at the narrow side related to the mucosal congestion and decongestion are of reduced amplitude. When the narrow side is in the "working" phase, NR is insusceptible to the mucosal decongestion and remains high. Simultaneous mucosal congestion on the opposite wide nasal passage normally increases NR that results in bilaterally high NR and consequently reduced patency of both nasal passages.

Conversely, mucosal decongestion decreases NR on the wide side allowing it to become dominant for breathing, whereas high NR at the narrow side is now even more accentuated due to mucosal congestion. The latter would result in a more significant reduction of airflow at the narrow side than normally expected in the "resting" phase of the nasal cycle. Besides, this would result in periodic fluctuations of the total NR that could contribute to the subjective sensation of the NAO.

Like other CFD studies, the current study might be limited by assumptions used in computational modeling. Since NR generates during inspiration[27], we simulated only an inspiratory airflow. As demonstrated by Chung et al.[28] and Lee et al.[29], modeling of steady flow is reliable to reveal important airflow features when compared to unsteady models[28,29]. A limitation that could arise from modeling of non-deformable nasal walls can be considered as a relative. A nasal wall deformation during inspiration, such as a nasal valve collapse, could not be expected since it occurs during much higher airflow rates (>500 ml/s) than that used in our study[30]. Moreover, none of our patients had diagnosed an inspiratory nasal valve collapse.

5. CONCLUSION

The current study provided a novel aspect of the NSD investigation by connecting NAO symptoms and side asymmetry in NR that occurs during nasal cycle phase changes. We revealed various degrees of side asymmetry in NR in different NSD types that may explain differences in NAO severity. NSD types located in the INV area (type 1 and 2) or those that contained an anterior component in this region (type 4 and 7 in our case) showed the greatest side asymmetry in NR as well as high NOSE scores.

REFERENCES

1. Cole P, Chaban R, Naito K, Oprysk D. The obstructive nasal septum. Effect of simulated deviations on nasal airflow resistance. Arch Otolaryngol Head Neck Surg 1988;114(4):410-412.
2. Haavisto LE, Sipila JI. Acoustic rhinometry, rhinomanometry and visual analogue scale before and after septal surgery: a prospective 10-year follow-up. Clin Otolaryngol 2013;38(1):23-29.
3. Andre RF, Vuyk HD, Ahmed A, Graamans K, Nolst Trenite GJ. Correlation between subjective and objective evaluation of the nasal airway. A systematic review of the highest level of evidence. Clin Otolaryngol 2009;34:518-525.
4. Onerci MT. Nasal physiology and pathophysiology of nasal disorders. Heidelberg: Springer; 2013. 259 p.
5. Dinis PB, Haider H. Septoplasty: Long-term evaluation of results. Am J Otolaryngol 2002;23:85-90.
6. Chen XB, Lee HP, Chong VF, Wang de Y. Assessment of septal deviation effects on nasal airflow: a computational fluid dynamics model. Laryngoscope 2009;119(9):1730-1736.

7. Radulesco T, Meister L, Bouchet G, Varoquaux A, Giordano J, Mancini J, Dessi P, Perrier P, Michel P. Correlations between computational fluid dynamics and clinical evaluation of nasal airway obstruction due to septal deviation: An observational study. Clin Otolaryngol 2019;44(4):603-611.
8. Wen J, Inthavong K, Tu J, Wang S. Numerical simulations for detailed airflow dynamics in a human nasal cavity. Respir Physiol Neurobiol 2008;161(2):125-135.
9. Garcia GJM, Rhee JS, Senior BA, Kimbell JS. Septal deviation and nasal resistance: an investigation using virtual surgery and computational fluid dynamics. Am J Rhinol Allergy 2010;24(1):46-53.
10. Kim SK, Heo GE, Seo A, Na Y, Chung SK. Correlation between nasal airflow characteristics and clinical relevance of nasal septal deviation to nasal airway obstruction. Respir Physiol Neurobiol 2014;192:95-101.
11. Hildebrandt T, Goubergrits L, Heppt WJ, Bessler S, Zachow S. Evaluation of the intranasal flow field through computational fluid dynamics. Facial Plast Surg 2013;29(2):93-98.
12. Kimbell JS, Garcia GJM, Frank DO, Cannon DE, Pawar SS, Rhee JS. Computed nasal resistance compared with patient-reported symptoms in surgically treated nasal airway passages: a preliminary report. Am J Rhinol Allergy 2012;26(3):94-98.
13. Janovic N, Maric G, Dusanovic M, Janovic A, Pekmezovic T, Djuric M. Introducing Nasal Obstruction Symptom Evaluation (NOSE) scale in clinical practice in Serbia: validation and cross-cultural adaptation. Vojnosanit Pregl 2018; doi.org/10.2298/VSP180619130J.
14. Mladina R, Cujic E, Subaric M, Vukovic K. Nasal septal deformities in ear, nose, and throat patients: An international study. Am J Otolaryngol 2008;29:75-82.
15. Poetker DM, Rhee JS, Mocan BO, Michel MA. Computed Tomography Technique for Evaluation of the Nasal Valve. Arch Facial Plast Surg. 2004; 6: 240-243.
16. Juretic F. cfMesh user guide. Document version: 1.1, Creative Fields, Zagreb, 2015 http://cfmesh.com/wp-content/uploads/2015/09/User_Guide-cfMesh_v1.1.pdf
17. Hall RL. Energetics of nose and mouth breathing, body size, body composition, and nose volume in young adult males and females. Am J Hum Biol 2005;17(3):321-330.

18. Menter FR. Two-equation eddy-viscosity turbulence models for engineering application. AIAA Journal 1994;32(8):1598-1605.
19. Borojeni AAT, Garcia GJM, Moghaddam MG, Frank-Ito DO, Kimbell JS, Laud PW, Koeniq LJ, Ree JS. Normative ranges of nasal airflow variables in healthy adults. Int J Comput Assist Radiol Surg 2020;15(1):87-98.
20. Rhee JS, Cannon DE, Frank DO, Kimbell JS. Role of virtual surgery in preoperative planning: assessing the individual components of functional nasal airway surgery. Arch Facial Plast Surg 2012;14(5):354-359.
21. Rhee JS, Pawar SS, Garcia GJ, Kimbell JS. Toward personalized nasal surgery using computational fluid dynamics. Arch Facial Plast Surg 2011;13(5):305-310.
22. Pendolino AL, Lund VJ, Nardello E, Ottaviano G. The nasal cycle: a comprehensive review. Rhinology 2018;1:67-76.
23. Cole P. Stability of nasal airflow resistance. Clin Otolaryngol Allied Sci 1989;14:177-182.
24. Fisher EW, Liu M, Lung VJ. The nasal cycle after deprivation of airflow: a study of laryngectomy patients using acoustic rhinometry. Acta Otolaryngol 1994;114:443-446.
25. Williams M, Eccles R. A model for the central control of airflow patterns within the human nasal cycle. J Laryngol Otol 2016;130:82-88.
26. Eccles R. A role for the nasal cycle in respiratory defence. Eur Respir J 1996;9:371-376.
27. Cole P. Biophysics of nasal airflow: a review. Am J Rhinol 2000;14:245-249.
28. Chung SK, Son YR, Shin SJ, Kim SK. Nasal airflow during respiratory cycle. Am J Rhinol 2006; 20:379-384.
29. Lee JH, Na Y, Kim SK, Chung SK. Unsteady flow characteristics through a human nasal airway. Respir Physiol Neurobiol 2010;172:136-146.
30. Mlynski G. Impaired function of the upper respiratory tract. Restorative procedures for upper airway dysfunction, nasal breathing. Laryngorhinootologie 2005; 84:S101-117.

FIGURE CAPTIONS

Figure 1. 3D computational model of the nasal cavity with eight cross-sections selected in the following regions: (1) 1 cm from the nostrils, (2) the narrowest part of the INV region, (3) head of the inferior turbinate, (4) head of the middle turbinate, (5) ostiomeatal unit, (6) head of the superior turbinate, (7) choanae, and (8) nasopharynx (2 cm behind the choanae).

Figure 2. Pressure drop through the right and left nasal passage in eight CFD models

TABLES

Table 1. CT criteria for NSD classification into Mladina's categories.

NSD type	Description
I	vertical deformation in the internal nasal valve region without affecting physiologic valve angle
II	vertical deformation in the internal nasal valve region that decreases the valve angle
III	C-shaped deformation at the level of the head of the middle turbinate
IV	S-shaped deformation with an anterior curvature located in the region of the internal nasal valve
V	straight nasal septum with the unilateral bony spur
VI	intermaxillary bone wing on one side and an anterior basal septal crest on the opposite side
VII	a combination of the two or more NSD types mentioned above

Table 2. NOSE scores (mean ± standard deviation), airflow partitioning (%), and CFD-NR (Pa/(mL/s)) for normal nasal cavity and 7 NSD types, separately for the left and right side.

	No. of patients	**NOSE score**	**Airflow partitioning (%)**		**CFD-NR (**Pa/(mL/s))		
			Left	***Right***	***Left***	***Right***	Δ***NR***
No NSD	7	0	45.83	54.17	0.0136	0.0152	-0.0016
NSD							
Type 1	4	20.00 ± 15.81	43.37	56.63	0.0232	0.0088	0.0144
Type 2	2	45.00 ± 28.28	34.71	65.29	0.0180	0.0068	0.0112
Type 3	53	13.68 ± 17.55	53.39	46.61	0.0158	0.0126	0.0032
Type 4	25	17.00 ± 19.04	51.96	48.04	0.0074	0.0194	-0.0120
Type 5	59	18.39 ± 17.92	55.04	44.96	0.0160	0.0248	-0.0088
Type 6	5	14.00 ± 10.84	55.91	44.09	0.0290	0.0266	0.0024

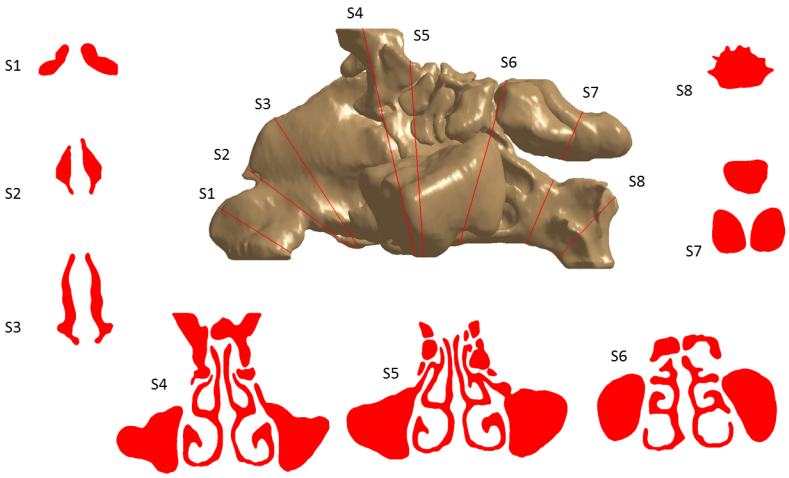

coa_13563_f1.tif

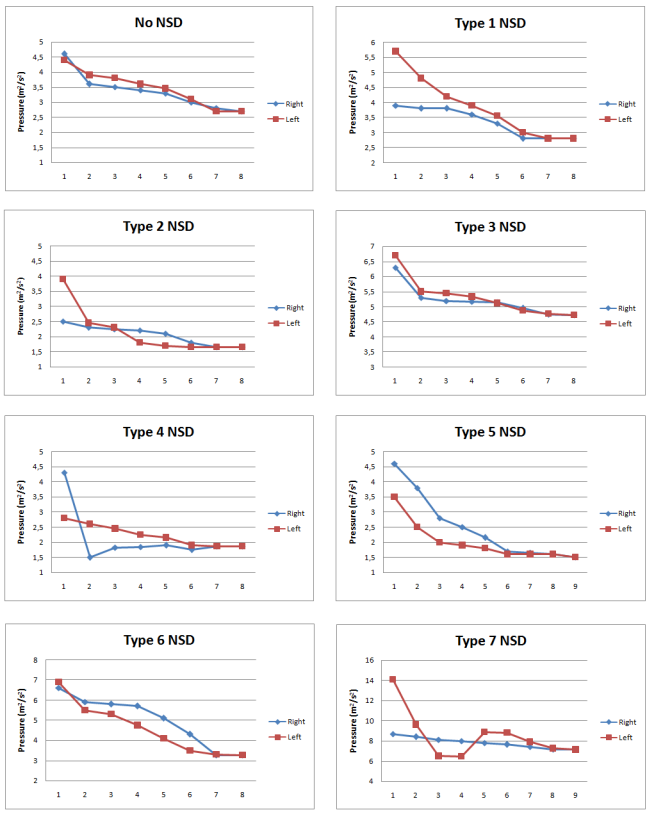

coa_13563_f2.tif